

Quantum quench dynamics of tilted dipolar bosons in 2D optical lattices

Hrushikesh Sable,^{1,2} Deepak Gaur,^{1,2} Soumik Bandyopadhyay,^{1,3} Rejish Nath,⁴ and D. Angom^{1,5}

¹*Physical Research Laboratory, Ahmedabad - 380009, Gujarat, India*

²*Indian Institute of Technology Gandhinagar, Palaj, Gandhinagar - 382355, Gujarat, India*

³*INO-CNR BEC Center and Department of Physics, University of Trento, Via Sommarive 14, I-38123 Trento, Italy*

⁴*Department of Physics, Indian Institute of Science Education and Research,
Dr. Homi Bhabha Road, Pune 411008, Maharashtra, India*

⁵*Department of Physics, Manipur University, Canchipur - 795003, Manipur, India*

(Dated: November 28, 2021)

We investigate the quench dynamics of the dipolar bosons in two dimensional optical lattice of square geometry using the time dependent Gutzwiller method. The system exhibits different density orders like the checkerboard and the striped pattern, depending upon the polarization angle of the dipoles. We quench the hopping parameter across the striped density wave (SDW) to striped supersolid (SSS) phase transition, and obtain the scaling laws for the correlation length and topological vortex density, as function of the quench rate. The results are reminiscent of the Kibble-Zurek mechanism (KZM). We also investigate the dynamics from the striped supersolid phase to the checkerboard supersolid phase, obtained by quenching the dipole tilt angle θ . This is a first order structural quantum phase transition, and we study the non-equilibrium dynamics from the perspective of the KZM. In particular, we find the number of the domains with checkerboard order follows a power law scaling with the quench rate. This indicates the applicability of the KZM to this first order quantum phase transition.

I. INTRODUCTION

A cornerstone of our understanding of the non-equilibrium dynamics across the continuous phase transitions is the Kibble-Zurek mechanism (KZM). The KZM provides a theoretical understanding of the spontaneous symmetry breaking across the continuous phase transitions, and predicts universal scaling laws of the relevant physical quantities, as a function of the quench rate [1–6]. The central idea is the breakdown of the adiabaticity near the critical point due to the critical slowing down. This implies that however slowly the system is quenched across the critical point, the dynamics ceases to be adiabatic, leading to the topological defects. In the context of cosmology, Kibble predicted the formation of the topological defects as a result of local choices of broken symmetry state in the phase transitions [1, 2]. Later, in a novel work Zurek identified the role of the critical slowing down in the creation of the topological defects in condensed matter systems like He⁴ [3, 4]. He also predicted the scaling laws for the correlation length and the defect density as a function of the quench rate. The prediction has been experimentally verified with the topological defects in the superfluid helium [7, 8]. Since then, the KZM has been studied in a wide variety of systems such as liquid crystals [9, 10], superconducting loops [11], ferroelectrics [12]. Initially developed for the classical phase transitions, the KZM was later applied to the quantum phase transitions (QPT)s.

In regard to the quantum phase transitions, one of the most well-studied systems are the ultracold atomic gases loaded in optical lattices. These systems are considered as the macroscopic quantum simulators of the condensed matter systems [13, 14]. A prototypical example of a quantum phase transition studied using these systems is the Mott Insulator (MI) to superfluid (SF) phase transition [15–18]. The ultracold atoms in optical lattice simulate the Bose-Hubbard model (BHM) [15, 16], which is a minimal model to study the physics of in-

teracting bosons in a lattice. These systems are used to understand various equilibrium quantum phases [19–28], collective excitations [29–34] etc. In the context of the KZM, there are many works done using the system of ultracold atoms. The early investigations in the ultracold atoms were for harmonic trapping potentials [35–43]. The experimental investigations of the dynamics of the QPT from the MI phase to the SF phase have been studied [44–46]. On the theoretical front, there have been works in investigating the evolution of the ground states during the quench process [6, 47–54].

The first order phase transitions are different from the second order phase transitions. They are characterized by the co-existence of multiple phases at the transition point. A natural extension of the KZM physics is to check its applicability to the first order phase transitions. Following this, there are few works [55, 56] which have studied the scaling of the topological defects in quenches across the first order phase transitions. And recently, there are experimental works [57, 58] that have shown the existence of the Kibble-Zurek (KZ) scaling across the first order phase transitions, in spinor condensates. Motivated by this, we also investigate the quench dynamics across a first order phase transition, in the system of dipolar bosons in 2D square lattice.

In this work, we consider the dipolar bosons in the two-dimensional square optical lattice. The anisotropy of the dipolar interactions between the bosons induce different density orders like checkerboard and striped in the system, depending on the polarization of the dipoles. To validate the predictions of the KZM for the dipolar bosons, we first consider quenching the hopping amplitude across the striped density wave to striped supersolid. We investigate the scaling laws, predicted in the KZM, for this second order quantum phase transition, and obtain the critical exponents of the correlation length and the topological defects. Then, the polarization of the dipoles is quenched so that the system is driven from the striped supersolid to checkerboard supersolid phase. We show the ex-

istence of the impulse and adiabatic domains in the dynamics across this first order phase transition, and calculate the number of domains of the checkerboard order generated during the quench. This number obeys a universal power-law scaling with the quench rate, an example of the KZM.

We have organized the remainder of this article as follows. In Sec. II we describe the model considered for our study and in the Sec. III we discuss about the theoretical methods we have used. We provide a description of the single-site mean-field theory used to obtain the equilibrium ground state phases and the quenched state. The results from the quench dynamics of the hopping parameter J and the tilt angle θ are then presented in Sec. IV. In Sec. V, we summarize the key results.

II. THEORETICAL MODEL

We consider a system of dipolar bosons in 2D optical lattice of square geometry with the lattice constant a . The lattice plane constitutes the x - y plane of the chosen co-ordinate system of the model, as shown schematically in the Fig. 1. At zero temperature, the physics of the system is well described by the lowest band BHM with the dipolar interaction and the Hamiltonian of the system is [19, 24, 59–61]

$$\hat{H} = - \sum_{\langle i,j \rangle} J \left(\hat{b}_i^\dagger \hat{b}_j + \text{H.c.} \right) + \sum_i \hat{n}_i \left[\frac{U}{2} (\hat{n}_i - 1) - \mu \right] + \frac{C_{\text{dd}}}{2} \sum_{ij} \hat{n}_i \hat{n}_j \frac{(1 - 3\cos^2 \alpha_{ij})}{|\mathbf{r}_i - \mathbf{r}_j|^3}, \quad (1)$$

where $i \equiv (p, q)$ represent the lattice indexes, and $j \equiv (p', q')$ are it's nearest neighbouring lattice site indexes, \hat{b}_i^\dagger (\hat{b}_i) are the creation (annihilation) operators, \hat{n}_i is the bosonic occupation number operator and the summation indexes within $\langle \dots \rangle$ denote the sum over the nearest neighbours. Further, J is the hopping strength, $U > 0$ is the on-site inter-atomic interaction strength, and μ is the chemical potential. The coupling constant $C_{\text{dd}} \propto d^2/a^3$ represents the strength of the dipolar interaction. Here, d represents the magnitude of either the permanent magnetic dipole moment, which atoms like Cr, Er and Dy possess, or electric dipole moment in the case of polar molecules. The angle α_{ij} is the angle between the polarization axis and the separation vector $\mathbf{r}_i - \mathbf{r}_j$. The long range and the anisotropic nature of the dipolar interaction induce various symmetry broken phases. In our study, for simplicity, we consider the model where the dipolar interaction is restricted to the NN sites. This is an optimal model which encapsulates the physics of the long range dipolar interactions of ultracold atoms in a lattice. Then the Hamiltonian is

$$\hat{H} = - \sum_{\langle i,j \rangle} J \left(\hat{b}_i^\dagger \hat{b}_j + \text{H.c.} \right) + \sum_i \hat{n}_i \left[\frac{U}{2} (\hat{n}_i - 1) - \mu \right] + \frac{C_{\text{dd}}}{2} \sum_{\langle ij \rangle} \hat{n}_i \hat{n}_j (1 - 3\cos^2 \alpha_{ij}). \quad (2)$$

The dipoles are assumed to be polarized in the y - z plane, as demonstrated in Fig. 1. The angle between the z -axis and

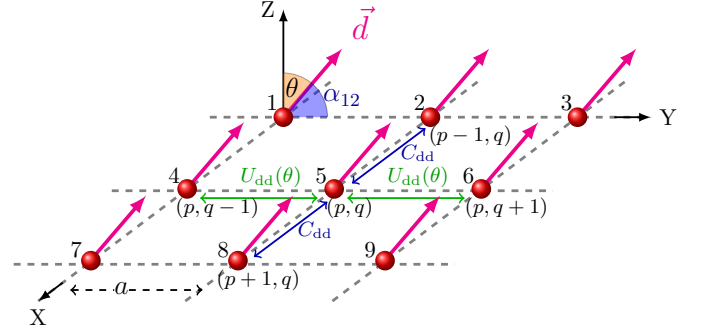


FIG. 1. The schematic of the dipolar bosons in 2D optical lattice. The lattice is in the x - y plane, and the polarization of the dipoles is in the y - z plane. The angle between the direction of the dipole moment \vec{d} and the z axis is the tilt angle θ , as is illustrated by the orange-shaded color. The dipolar interaction between the nearest neighbouring dipoles along the x direction is represented by C_{dd} , while the interaction along the y direction is given by $U_{\text{dd}}(\theta)$.

the polarization axis is denoted by θ , and is referred to as the tilt angle. The tilt angle can be experimentally controlled by applying an external electric and magnetic field for the electric and magnetic dipoles, respectively. In this work, we consider the atoms with magnetic dipole moment, as these are primarily used in experiments on dipolar Bose-Einstein condensates (BECs) [62]. Since the polarization is in the y - z plane, it should be noted that $\theta = \pi/2 - \alpha_{ij}$. The isotropic limit of the model is obtained when $\theta = 0$, and this is commonly referred to as the extended BHM (eBHM) [21, 26]. For the configuration considered, the dipole-dipole interaction along the x -axis is always repulsive and independent of θ . Along the y -axis the interaction is θ dependent and it has form $U_{\text{dd}}(\theta) = C_{\text{dd}}(1 - 3\sin^2 \theta)$. The interaction along the y -axis is repulsive when $\theta < \theta_M$, and attractive for $\theta > \theta_M$, where $\theta_M = \sin^{-1}(1/\sqrt{3}) \approx 35.3^\circ$, is referred to as the magic angle. At the magic angle, the dipole interaction along the y -axis is zero. In the present work, we first focus on the case $\theta > \theta_M$, and study the interplay of the attractive $U_{\text{dd}}(\theta)$ with the repulsive U and the dipolar interaction along x -axis. Then, we tune the tilt angle θ across the magic angle θ_M and study the structural phase transition between the striped supersolid phase and the checkerboard supersolid phase.

III. THEORETICAL METHODS

A. Single site Gutzwiller mean-field (SGMF) theory

We use the SGMF method to obtain the ground state of the model. In this method, the annihilation (creation) operators at lattice site (p, q) in Eq.(2) are decomposed as [21–25, 27, 28, 63, 64]

$$\hat{b}_{p,q} = \phi_{p,q} + \delta \hat{b}_{p,q}, \quad (3a)$$

$$\hat{b}_{p,q}^\dagger = \phi_{p,q}^* + \delta \hat{b}_{p,q}^\dagger \quad (3b)$$

where, $\phi_{p,q} = \langle \hat{b}_{p,q} \rangle$, and $\phi_{p,q}^* = \langle \hat{b}_{p,q}^\dagger \rangle$ are the mean field and its complex conjugate, respectively. Here the expectation values are taken with respect to the ground state of the system. A similar application is done to the number operator $\hat{n}_{p,q}$ and then, we can write the single-site mean field Hamiltonian as

$$\hat{h}_{p,q} = \hat{h}_{p,q}^{\text{BHM}} + \hat{h}_{p,q}^x + \hat{h}_{p,q}^y, \quad (4)$$

where, the single-site Bose-Hubbard model Hamiltonian is

$$\begin{aligned} \hat{h}_{p,q}^{\text{BHM}} = & -J \left[\left(\phi_{p+1,q}^* \hat{b}_{p,q} - \phi_{p+1,q} \phi_{p,q} + \right. \right. \\ & \left. \left. \phi_{p,q+1}^* \hat{b}_{p,q} - \phi_{p,q+1} \phi_{p,q} \right) + \text{H.c.} \right] \\ & + \frac{U}{2} \hat{n}_{p,q} (\hat{n}_{p,q} - 1) - \mu_{p,q} \hat{n}_{p,q}, \end{aligned} \quad (5)$$

the single-site mean field Hamiltonian arising from the long range interaction along x -axis is

$$\hat{h}_{p,q}^x = \frac{C_{\text{dd}}}{2} \sum_{p'} \left(\langle \hat{n}_{p',q} \rangle \hat{n}_{p,q} - \langle \hat{n}_{p',q} \rangle \langle \hat{n}_{p,q} \rangle \right), \quad (6)$$

with $p' = p - 1$ and $p + 1$. Similarly, for the long range interaction along the y -axis, the single-site mean field Hamiltonian is

$$\hat{h}_{p,q}^y = \frac{U_{\text{dd}}(\theta)}{2} \sum_{q'} \left(\langle \hat{n}_{p,q'} \rangle \hat{n}_{p,q} - \langle \hat{n}_{p,q'} \rangle \langle \hat{n}_{p,q} \rangle \right), \quad (7)$$

with $q' = q - 1$ and $q + 1$. The total mean field Hamiltonian of the system is then,

$$\hat{H}^{\text{MF}} = \sum_{p,q} \hat{h}_{p,q}. \quad (8)$$

Using the Gutzwiller ansatz, the ground state of the system is

$$|\Psi_{\text{GW}}\rangle = \prod_{p,q} |\psi\rangle_{p,q} = \prod_{p,q} \sum_{n=0}^{N_b} c_n^{(p,q)} |n\rangle_{p,q}, \quad (9)$$

where, N_b is the maximum allowed occupation number basis (Fock space basis), and $c_n^{(p,q)}$ are the coefficients of the occupation number state $|n\rangle$ at the lattice site (p, q) . The SF mean-field order parameter $\phi_{p,q}$ is calculated as

$$\phi_{p,q} = \langle \Psi_{\text{GW}} | \hat{b}_{p,q} | \Psi_{\text{GW}} \rangle = \sum_{n=1}^{N_b} \sqrt{n} c_{n-1}^{(p,q)*} c_n^{(p,q)}. \quad (10)$$

The occupancy at a lattice site (p, q) is the expectation of the number operator

$$\langle \hat{n}_{p,q} \rangle = \sum_{n=0}^{N_b} |c_n^{(p,q)}|^2 n_{p,q}. \quad (11)$$

Since the mean field Hamiltonian depends on ϕ and $\langle \hat{n} \rangle$, which are the expectation values of single-site operators, we

initialize their values by choosing a specific local wavefunction. In general, we choose the single site wavefunction such that $c_n^{(p,q)}$ have the same magnitude, and normalize it. We, then, solve for the ground state of each site by diagonalizing the corresponding single site Hamiltonian. And, recalculate the SF order parameter and the expectation of the number operator. This is done for all of the lattice sites and one such sequence of calculation constitutes one iteration. The iterations are repeated till we achieve convergence.

B. Characterization of quantum phases

The quantum phases of the dipolar BHM are identified by a unique combination of different order parameters. The ground state of the standard BHM exhibits two quantum phases: Mott insulator (MI) and the superfluid (SF) phase. The MI phase is an insulating phase, and has fixed, integer commensurate lattice site occupancies. The SF phase is a compressible phase, and displays the characteristic off-diagonal long range order (ODLRO). The SF order parameter ϕ is zero in the MI phase, and is finite in the SF phase. Thus, ϕ is an order parameter which distinguish the two quantum phases of the standard BHM. For ultracold dipolar atoms in an optical lattice, the long range interactions introduce additional quantum phases. These are structured phases like the density-wave (DW) and the supersolid (SS) phases. These phases have diagonal long-range crystalline order. The SS phase, in addition, has ODLRO. Hence, it has non-zero ϕ and periodic modulation of $\langle \hat{n}_{p,q} \rangle$. The periodic modulation of the density is captured by the structure factor $S(\mathbf{k})$ [24], where $\mathbf{k} = k_x \hat{i} + k_y \hat{j}$ is the two-dimensional reciprocal lattice vector,

$$S(\mathbf{k}) = \frac{1}{N^2} \sum_{i,j} e^{i\mathbf{k} \cdot (\mathbf{r}_i - \mathbf{r}_j)} \langle \hat{n}_i \hat{n}_j \rangle, \quad (12)$$

and N is the total number of bosons in the lattice. As mentioned earlier, we first consider $\theta > \theta_M$ domain and study the hopping quenching. Then the associated anisotropy of the long range interaction induces the periodic density modulations along the x -axis, since the interaction along the y -axis is attractive. Hence, for $(k_x, k_y) = (\pi, 0)$, $S(\mathbf{k})$ is non-zero in the DW and the SS phases. This implies that the translational symmetry is broken along the x direction. Henceforth, we shall be referring to these quantum phases as striped density wave SDW (n_A, n_B) and striped supersolid (SSS) phases in our study. Here, n_A and n_B are the occupancies of the two consecutive lattice sites along the x direction. For $\theta < \theta_M$, the dipolar interaction induces periodic density modulation along both the x and y directions. The quantum phases then have checkerboard order, and are referred as checkerboard density wave (CBDW) and checkerboard supersolid (CBSS) phases. We use $S(\pi, \pi)$ to identify these ordered phases. This implies that these checkerboard phases break the translational symmetry along both the directions. Table I summarizes the classification of all the quantum phases discussed in the present work.

| Quantum phases | $n_{p,q}$ | $\phi_{p,q}$ | $S(\pi, 0)$ | $S(\pi, \pi)$ |
|----------------------------------|-----------|--------------|-------------|---------------|
| Mott insulator (MI) | Integer | 0 | 0 | 0 |
| Striped Density wave (SDW) | Integer | 0 | $\neq 0$ | 0 |
| Striped Supersolid (SSS) | Real | $\neq 0$ | $\neq 0$ | 0 |
| Checkerboard Density wave (CBDW) | Integer | 0 | 0 | $\neq 0$ |
| Checkerboard Supersolid (SSS) | Real | $\neq 0$ | 0 | $\neq 0$ |
| Superfluid (SF) | Real | $\neq 0$ | 0 | 0 |

TABLE I. Classification of quantum phases based on different order parameters.

C. Quench dynamics and KZ scaling relations.

In this work we study the dynamics of the system when a chosen parameter χ undergoes quantum quench from an initial value χ_i to a final value χ_f , here χ is either J or θ . During the quench the parameter is a function of time $\chi(t)$ and modifies the Hamiltonian in Eq.(8) to a time dependent one. The other parameters C_{dd} , U and μ remain fixed or time independent. Then, the time-dependent Schrodinger equation

$$i\hbar\partial_t |\psi\rangle_{p,q} = \hat{h}_{p,q} |\psi\rangle_{p,q}, \quad (13)$$

describes the temporal evolution of the single site wavefunction. This results to a set of coupled, linear partial differential equations of the coefficients $c_n^{(p,q)}(t)$. To solve these equations we employ the fourth-order Runge-Kutta method and once we have $c_n^{(p,q)}(t)$ the wavefunction of the system at a particular instant of time t is defined. To initiate the quantum quench, we obtain the equilibrium wavefunction with the $\chi = \chi_i$. In the next step of the state preparation for the quantum quench dynamics, we introduce fluctuations to the coefficients $c_n^{(p,q)}$ of this state. For the J quenching, we introduce phase and density fluctuations. The phase fluctuations are introduced to the non-zero coefficients of the wavefunction. For this we generate uni-variate random phases in the domain $[0, 2\pi]$. We, then, introduce density fluctuations by adding noise to the amplitudes of the coefficients $c_n^{(p,q)}$. This is done by generating uni-variate random numbers in the domain $[0, \Delta]$, with $\Delta \approx 10^{-4}$. In the case of the θ quenching, the density fluctuations alone is sufficient to drive the SSS-CBSS transition as it involves a change in the density order. The choice of the strength Δ is based on a detailed analysis of the quantum and thermal fluctuations using Bogoliubov-de Gennes analysis of the collective modes, see Appendix A. These fluctuations simulate the effects of the quantum fluctuations in the system, and are essential to drive the quantum phase transitions. To obtain reliable statistics, we consider an ensemble consisting of 80 such randomized initial states. And, each of these states are evolved in time by quenching the appropriate parameter. Then, a measure of a physical observable is the ensemble average over all the 80 samples. Furthermore, for each member of the ensemble we consider the average value of the observable across the entire system. For example, to examine the quench dynamics of the SF order pa-

rameter, we consider the system average

$$|\Phi| = \frac{\sum_{p,q} |\phi_{p,q}|}{N_s}, \quad (14)$$

as a representative value and here, N_s is the total number of lattice sites in the system.

There are several important temporal markers in a quantum quench dynamics. The Kibble-Zurek mechanism categorizes the entire quench process into three temporal regimes [65, 66]. Assuming that the quench is linear and is initiated at time $t = -\tau_Q$, the time duration $[-\tau_Q, -\hat{t}]$ marks the adiabatic regime. As the name suggests, in this temporal regime, the relaxation time τ of the system is short and the system adjusts to the temporal change in the parameter. In other words, τ is smaller than the time scale on which the quench is performed. As the system approaches the quantum critical point at $t = 0$, τ diverges, and dynamics is frozen. That is, the state of the system cannot follow the change in the parameter. This scenario persists till the time \hat{t} , and the time duration $[-\hat{t}, \hat{t}]$ marks the impulse period of the quench. The time instant \hat{t} is generally referred to as the transition time, and the rate of the quench is $1/\tau_Q$. For $t > \hat{t}$, the system is again in the adiabatic regime.

The Kibble-Zurek theory [1–5] predicts the rate of the topological defects formation during the course of the non-equilibrium dynamics. These defects are generated due to the different local choices of the order parameter associated with the symmetry broken phase. The symmetry breaking occurs spontaneously and the system undergoes a quantum phase transition as it crosses the critical point at $t = 0$. For an extended system, the choice of the broken symmetry must propagate across the entire system for it to be uniform. But, depending on the rate governed by τ_Q , this is forbidden, and finite sized domains are formed in the system. In other words, the formation of these domains is a direct consequence of causality [4]. In the case of the J quenching, which results in spontaneous breaking of global $U(1)$ symmetry, the defects manifest as vortices, and we compute their density as follows [52, 53, 55]:

$$N_v = \sum_{p,q} |\Omega_{p,q}|, \quad (15)$$

with

$$\Omega_{p,q} = \frac{1}{4} [\sin(\theta_{p+1,q} - \theta_{p,q}) + \sin(\theta_{p+1,q+1} - \theta_{p+1,q}) - \sin(\theta_{p+1,q+1} - \theta_{p,q+1}) - \sin(\theta_{p,q+1} - \theta_{p,q})]. \quad (16)$$

Here, $\theta_{p,q}$ is the phase of the SF order parameter $\phi_{p,q}$. For large τ_Q , the quench rate is small, and the number of the vortices N_v is small. Thus, N_v satisfies the scaling law

$$N_v \propto \tau_Q^{-d}, \quad (17)$$

where, d is the critical exponent. We also compute the correlation length ξ [52, 53, 55], which captures the correlation between the lattice sites of the system. It is defined as

$$\langle b_i^\dagger b_j \rangle \propto \exp\left(\frac{-|i-j|}{\xi}\right). \quad (18)$$

For a given pair $\{i, j\}$ of lattice sites, we invert the above relation to calculate ξ for the pair. We then average this quantity over all possible pairs in the lattice, and this also covers all possible spatial separations. The scaling law of ξ is

$$\xi \propto \tau_Q^b,$$

where, b is the critical exponent. The critical exponents b and d are related to the other critical exponents ν and z as

$$b = \frac{\nu}{1 + \nu z} \quad (19a)$$

$$d = \frac{2\nu}{1 + \nu z}. \quad (19b)$$

Here, ν is the critical exponent of the equilibrium correlation length and z is the dynamical critical exponent. Thus, the KZ mechanism predicts the scaling relation $d = 2b$. In the present work, one of our aim is to validate this scaling relation for the quantum phase transition from the SDW phase to SSS phase. For the θ quench across the SSS-CBSS transition, domains of the checkerboard order emerge during the dynamics. Analogous to the defect density, we quantify the number of domains N_D , and obtain a power-law scaling of it with the quench rate.

IV. RESULTS

When the tilt angle θ is greater than θ_M , the magic angle, the density wave (DW) and supersolid (SS) phases have striped order along the y -axis. This configuration is energetically favourable as the NN dipolar interaction along the y direction is attractive for $\theta > \theta_M$ and the dipoles are aligned head-to-tail formation. We first consider $\theta = 40^\circ$ and study the quantum quench from striped density wave (SDW(1,0)) to striped supersolid (SSS). This θ value is chosen so that the system is deep in the striped domain, and avoids the instabilities associated with large θ . We present the equilibrium phase diagram for the dipolar BHM at $\theta = 40^\circ$, in the J/U - μ/U plane obtained using the SGMF method. After verifying the KZ scaling relations for the SDW(1,0) to SSS transition, we consider the θ quench across the SSS-CBSS phase transition. We verify the presence of the impulse and adiabatic domains in the dynamics, and quantify the domains of the emerging checkerboard order. We consider the system size as 100×100 in our computations. We scale the Hamiltonian with U and time is defined in the units of \hbar/U .

A. Equilibrium phase diagram

The ground state phase diagram of the Hamiltonian with anisotropic NN interaction, given by Eq.(2), is shown in Fig. 2 for $\theta = 40^\circ$. At low values of J/U or in the strongly interacting domain, the ground state of the system is in the insulating SDW [20, 24] phase. The SDW phase, like the MI phase, is incompressible and has $\phi = 0$. The latter implies the absence of ODLRO in this phase. For large values of J/U , the system is in the SF phase and possess ODLRO. The SF phase

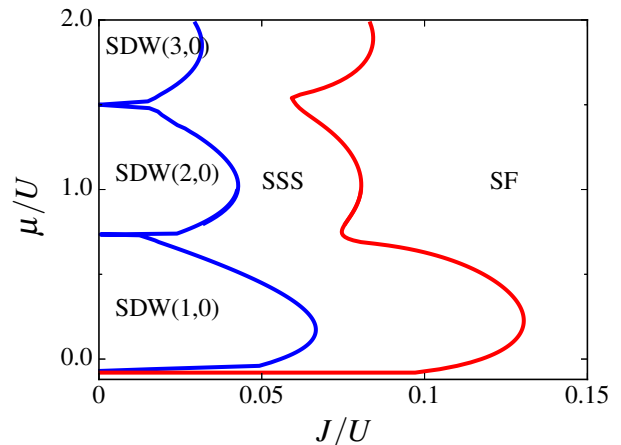


FIG. 2. Phase diagram of dipolar BHM for $\theta = 40^\circ$ in the J/U - μ/U plane. The blue line denotes the SDW - SSS phase boundary, while the red line denotes the SSS-SF phase boundary.

has translational invariance, and hence, it has $S(\pi, 0) = 0$. In the Fig. 3, the variation of the $S(\pi, 0)$ and $|\Phi|$ is shown as a function of J/U for $\mu/U = 0.17$. When the system is in the SDW(1,0) phase, the value of $S(\pi, 0)$ is unity and $|\Phi| = 0$. The domains of the two quantum phases SDW and SF are separated by the SSS phase. In the SSS phase, both the order parameters $S(\pi, 0)$ and $|\Phi|$ are non-zero. The structure of the occupancies in SSS phase are similar to the SDW phase, but, the occupancies are real. The SSS phase has both the ODLRO and diagonal long range order [20, 24, 67, 68]. Thus, the SDW and the SF phases are separated by two second-order phase transitions, SDW to SSS, and SSS to SF.

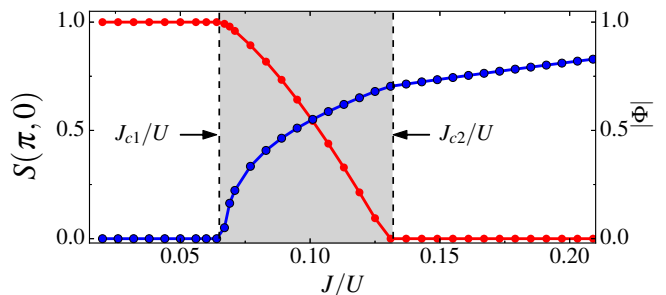


FIG. 3. $S(\pi, 0)$ (red) and $|\Phi|$ (blue) as a function of J/U , for $\mu/U = 0.17$. The black arrows mark the two transition points J_{c1}/U and J_{c2}/U , for the SDW to SSS and SSS to SF phase transition, respectively.

In the subsequent subsection, we study the dynamics of the second-order quantum phase transition from the SDW(1,0) phase to SSS phase, at fixed μ/U and C_{dd}/U .

B. Transition from SDW to SSS

To study the non-equilibrium SDW-SSS quantum phase transition, we employ the following linear quantum quench

protocol

$$J(t) = J_i + \frac{(J_c - J_i)}{\tau_Q}(t + \tau_Q). \quad (20)$$

With this protocol, we have, $J(-\tau_Q) = J_i$ and $J(0) = J_c$. For our study we take $J_i = 0.02U$ and $J_f = 0.11U$, and fix the chemical potential $\mu = 0.17U$. The value of the μ is chosen so that it corresponds to the tip of the SDW(1,0) lobe and $J_c = 0.067U$. Thus, at $t = -\tau_Q$, the system is in the SDW(1,0) phase, and at $t = t_f$, it is in the SSS phase when the quantum quench ends. The quench protocol employed in our simulations is shown in the Fig. 4(b), for $\tau_Q = 100$. Once the quench is terminated, we let the system evolve freely so that the order parameters attain steady values.

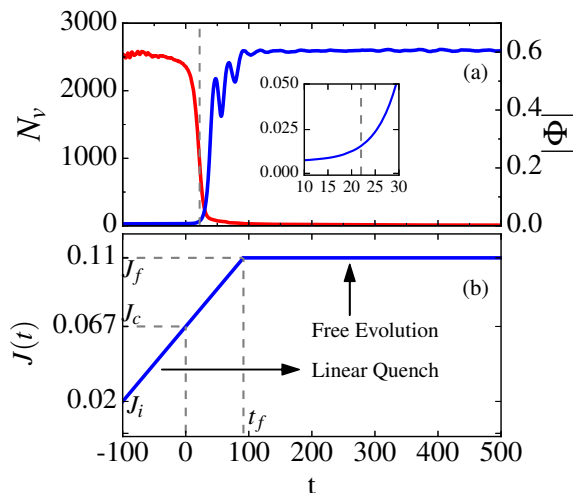


FIG. 4. The time evolution of $|\Phi|$ (blue) and N_v (red) for $\tau_Q = 100$ is shown in (a). The inset in (a) depicts the behaviour of $|\Phi|$ near \hat{t} . The critical point of the phase transition is passed at $t = 0$. The dashed line in (a) indicates the time \hat{t} , at which the SF order parameter rises steeply, as illustrated in the inset. As the system enters the SSS phase, there is an annihilation of the vortices and hence, N_v decreases to zero. In (b), we schematically illustrate the quench protocol used in our simulations. The hopping amplitude is ramped up from value J_i to J_c in time τ_Q (here $\tau_Q = 100$). After the quench is terminated at J_f , the system is freely evolved to attain a steady state.

1. $|\Phi|$

In the Fig. 4(a), we show the temporal evolution of $|\Phi|$ and N_v during the quantum quench for $\tau_Q = 100$. At the initial stages of the quantum quench, the SF order parameter is small $|\Phi| \approx 10^{-4}$ as the system passes through the SDW(1,0) phase domain. It is to be noted that, at equilibrium, $|\Phi|$ is zero in an insulating phase like SDW. However, in the quench dynamics it has a small value as the equilibrium solution is augmented with density and phase fluctuations during the initial state preparation. The value of $|\Phi|$ remains small after crossing the critical value J_c , at time $t = 0$, till the time \hat{t} . After time \hat{t} there is an initial exponential increase in the value of

$|\Phi|$. And, this is discernible from the inset plot in Fig. 4(a). At a later time, a damped oscillatory trend sets in while the average value tend towards the steady state value. For the present case, the quantum quench is terminated at $t_f = \tau_Q$, and then, we let the system evolve freely to attain a steady state. On the termination of the quantum quench, $|\Phi|$ stops increasing, and settles to its steady state value.

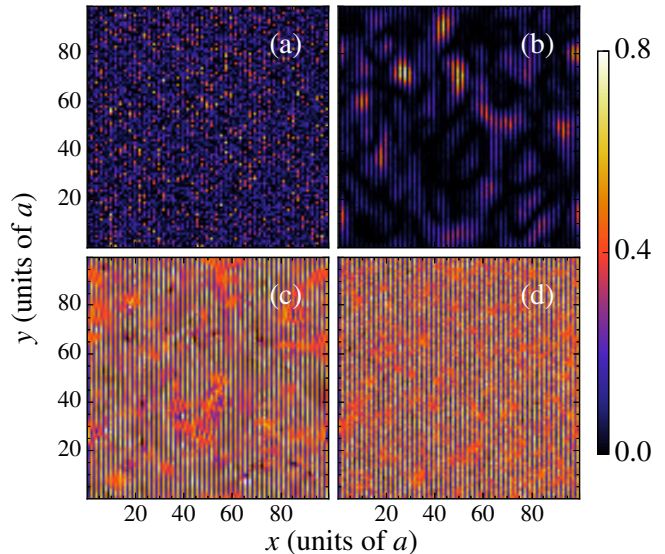


FIG. 5. Snapshots of $|\phi_{p,q}|$ at certain times for $\tau_Q = 100$. Initially at $t = -\tau_Q$, $|\phi_{p,q}|$ is small as shown in (a). As time progresses, the magnitude of $|\phi_{p,q}|$ increases as shown in (b). Plot (b) is at $t = \hat{t} = 28$. Domains of non-zero $|\phi_{p,q}|$ are formed at this time, and they grow in size, thereby increasing the value of $|\Phi|$. The representative progress of the phase ordering and domain merging can be seen in (c) and (d). Plot (c) is at $t = 92$, while plot (d) is at $t = 400$.

We present snapshots of $|\phi_{p,q}|$ at important time instants during the quench dynamics in the Fig. 5. At time $t = -\tau_Q$, as discussed earlier and visible in Fig. 5(a), $|\phi_{p,q}|$ has small value. Despite the small value the fluctuations in $|\phi_{p,q}|$ is evident from the figure. The delay in the transition to SSS phase till \hat{t} as the system evolves through the impulse domain is reflected in the value of $|\phi_{p,q}|$ shown in Fig. 5(b). In the figure, the emergence of few small SSS domains is visible as the system exits impulse domain and re-enters the adiabatic domain. This indicates there are local choices of the order parameter in the symmetry broken SSS phase. When the J/U is further increased, as discussed earlier and shown in the Fig. 4(a), $|\Phi|$ increases exponentially. At later times, the domains grow in size and phase ordering occurs. The representative progress of the phase ordering are shown in Fig. 5(c) and (d).

2. N_v

The vortex density N_v , as mentioned earlier, is an indicator of the defect density in the system. And, for a linear quench it satisfies the scaling law $N_v \propto \tau_Q^{-d}$. At initial stages of the quantum quench, the vortex density is high $N_v \approx 2500$.

This occurs as vortices are imprinted due to the phase fluctuations introduced during the initial state preparation. The $U(1)$ global symmetry of the system is broken spontaneously as the quantum quench progresses and enters the SSS phase after crossing the phase boundary. The SF order parameter $|\Phi|$, then, acquires a finite value and $\phi_{p,q}$ must be phase coherent throughout the system. However, in the quenched system, domains are formed such that there is phase coherence within, but not between the domains. At later times, the domains grow in size through mergers. This is accompanied by annihilation of vortex-antivortex pairs, and reduces the vortex density N_v in the system. As the quench is continued further, phase coherence is established in the system, and N_v approaches zero. Another observable which is an indicator of the

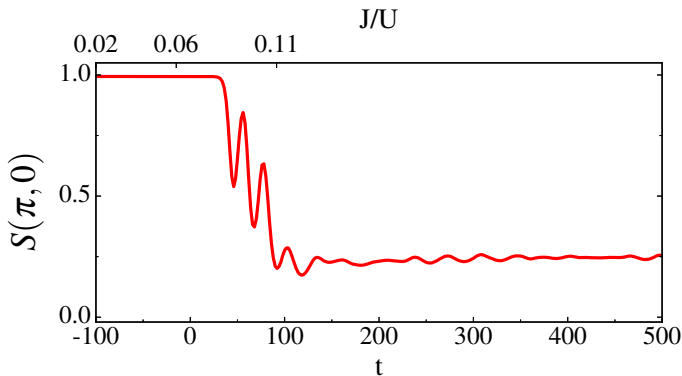


FIG. 6. $S(\pi, 0)$ as a function of time, for $\tau_Q = 100$. Since the SDW phase has crystalline property, $S(\pi, 0)$ equals unity in this phase. In the SSS phase, the solidity persists, but there is also superfluid character in the system, and $S(\pi, 0)$ deviates from unity. The hopping parameter J/U corresponding to time t is shown on the top axis. After the quench is terminated at $J_f = 0.11U$, the system is freely evolved with $J = J_f$.

SDW-SSS transition is the structure factor $S(\pi, 0)$. The evolution of the $S(\pi, 0)$ during the quantum quench dynamics is shown in Fig. 6. Like in the temporal evolution of $|\Phi|$, there is a significant change in the value of $S(\pi, 0)$ around the time \hat{t} . We observe that $S(\pi, 0)$ deviates from unity at \hat{t} , when few finite sized SF domains develops in the system. The domains display large amplitude oscillations while it continues to decay exponentially. Once the quantum quench is terminated and the system is in the free evolution stage, $S(\pi, 0)$ exhibits small amplitude oscillations about the steady state value.

To visualize the vortices in the system, the snapshots of the phase of the SF order parameter $\phi_{p,q}$ are shown in Fig. 7. In the figure, the location of a vortex (antivortex) is identified as the point around which the phase of $\phi_{p,q}$ change by 2π along anti-clockwise (clockwise) direction. At the beginning of the quantum quench $t = -\tau_Q$, as seen from Fig. 7(a), many vortices are present in the system. The appearance of the SF domains after the system crosses the critical point is visible in the Fig. 7(b), which shows the phase of $\phi_{p,q}$ at $t = \hat{t} = 28$. Two features are discernible in the figure. First, the phase coherence within each of the domains are indicated by the near uniform color. And, second, the presence

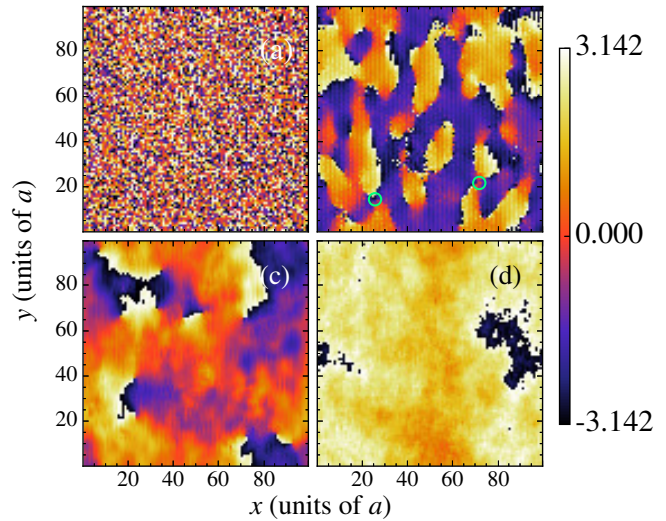


FIG. 7. Snapshots of the phase of $\phi_{p,q}$ at certain times for $\tau_Q = 100$. Initially at $t = -\tau_Q$, the vortex density is high, as shown in (a), owing to the phase fluctuations imprinted to the system. The domains of uniform phase are formed after the system crosses the critical point, as shown in (b), which is at $t = \hat{t} = 28$. As an illustration of the vortices in the system, we show two of them by the green circles. There is phase ordering process which increases the size of the domains and eventually system retains an almost uniform phase, as shown in (c) and (d). Plot (c) is at $t = 92$ and (d) is at $t = 400$.

of vortices at the points where more than two domains meet. The reduction in the number of vortices (antivortices) through vortex-antivortex annihilation is visible when we compare the plots at later times shown in Fig. 7(c-d). From the sequence of the plots, post \hat{t} , the consolidation of the domains size or phase ordering in the system is quite prominent. As seen from Fig. 7(d) at later times, the system has almost uniform phase.

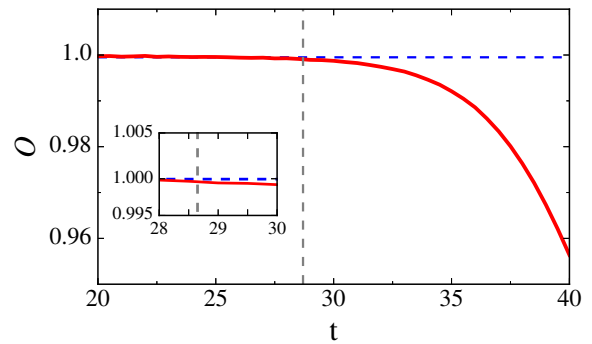


FIG. 8. Plot of the overlap measure $O(t)$, defined in Eq.(21), to locate \hat{t} . The red curve indicates the overlap, while the vertical grey dashed line indicates the time \hat{t} at which $O(t)$ begins to deviate from unity. The inset zooms into the region near \hat{t} . The dashed blue line is a visual guide to indicate the unity on the ordinate axis.

3. Protocol to locate \hat{t}

The scaling laws are applicable at the transition time \hat{t} and hence it is important to identify \hat{t} accurately. To locate \hat{t} , we compute the overlap of the wavefunction of the system at $t > 0$ with the wavefunction at $t = 0$ as

$$O(t) = |\langle \Psi(0) | \Psi(t) \rangle|. \quad (21)$$

As indicated earlier, the quantity $O(t)$ should be equal to unity as long as the system is in the impulse regime or $t \leq \hat{t}$. This follows as the state of the system remains frozen in the impulse regime. This is because the state maximally picks up a phase factor, when it is in the impulse domain[66]. At \hat{t} , when it passes from the impulse to adiabatic regime, the overlap shall start to deviate from unity. Thus, computing the $O(t)$, we locate the \hat{t} by noting the time at which it deviates from unity. As an example, Fig. 8 shows a generic plot of $O(t)$ around \hat{t} .

4. Critical exponents and scaling relations

To determine the critical exponents b and d , we do a series of computations over a range of τ_Q . The values of N_v and ξ obtained as a function of τ_Q are shown in Fig. 9(a-b). The critical exponents b and d obtained from these are 0.18 and 0.39, respectively. And, they approximately satisfy the scaling relation $d = 2b$ obtained from Eq. (19). The KZ mechanism also predicts the scaling law for the transition time

$$\hat{t} \propto \tau_Q^{\frac{\nu z}{1+\nu z}}, \quad (22)$$

and a plot of the \hat{t} as a function of τ_Q is shown in Fig. 9(c). Comparing with the expression of b in Eq. (19), we get $z \approx 2$. We have also studied the dynamics of the SDW(2,0)-SSS quantum phase transition. The quench protocol is similar to the case of SDW(1,0)-SSS transition. For a given τ_Q , we observe larger \hat{t} for the SDW(2,0)-SSS transition than the SDW(1,0)-SSS transition. From the results we get critical exponents as $b = 0.19$, and $d = 0.39$. Thus the critical exponents obey the scaling relation $d = 2b$.

C. Quenching θ

The dipolar gases in optical lattice offer an unique possibility of tuning the tilt angle θ , thereby control the anisotropy of the dipolar interactions. This leads to a rich equilibrium phase diagram of the system [20, 24]. The quenching of the tilt angle θ can be done in experiments by changing the orientation of the external magnetic field [62]. And, when θ is quenched across θ_M in our system, the dipolar interaction along the y -axis changes from repulsive to attractive. This leads to a first order quantum phase transition from the striped to checkerboard order. We study this first order phase transition from the perspective of the KZ mechanism. And, the same has been attempted in a few previous works. But, not all of them show the

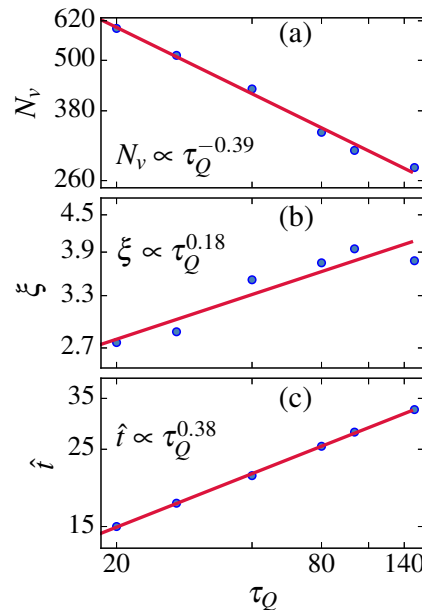


FIG. 9. Power law scaling of N_v , ξ and \hat{t} with respect to τ_Q . The exponent $d = 0.39$, $b = 0.18$ and the $\hat{t} \propto \tau_Q^{0.38}$. The obtained exponents b and d approximately satisfy the scaling relation $d = 2b$.

power-law scaling of the defect density with the quench rate. In [55], a power law dependence is obtained for the topological defects across the density wave-to-superfluid transition, while in [56], an exponential saturation of the defects is observed for the dynamics of a quantum search. In [57], the authors have considered quantum quench across the polar and the anti-ferromagnetic phases in spinor condensates, and have shown the presence of the adiabatic and the impulse domains in the evolution. They report the power-law scaling of the tuning parameter in the quench. It is thus pertinent to check for the presence of the impulse and adiabatic regimes in the dynamics of striped to checkerboard transition, and the associated power-law scalings.

1. Equilibrium ground state

For the quench dynamics, we fix the parameters of the system as $J = 0.05U$, and $\mu = 0.75U$. The corresponding critical tilt angle θ_c at which the SSS-CBSS quantum phase transition occurs is 35.3° , and thus $\theta_c \approx \theta_M$. As a first step to examine the quench dynamics we characterise the equilibrium ground state of the system as a function of θ . In particular, the kink in the energy per particle E/N of the ground state at the θ_c , as shown in Fig. 10(a), indicates a first order quantum phase transition. The system has striped order along y -axis (SSS phase) and checkerboard order for $\theta > \theta_c$ and $\theta < \theta_c$, respectively. The two quantum phases are discernible from the structure factors $S(\pi, \pi)$ and $S(\pi, 0)$. As shown in Fig. 10(b), $S(\pi, \pi)$ and $S(\pi, 0)$ are non-zero for the phases with checkerboard and striped order, respectively. In the neighbourhood of θ_M , the converged solutions are sensitive to the initial state. The most common solution is a metastable emulsion phase,

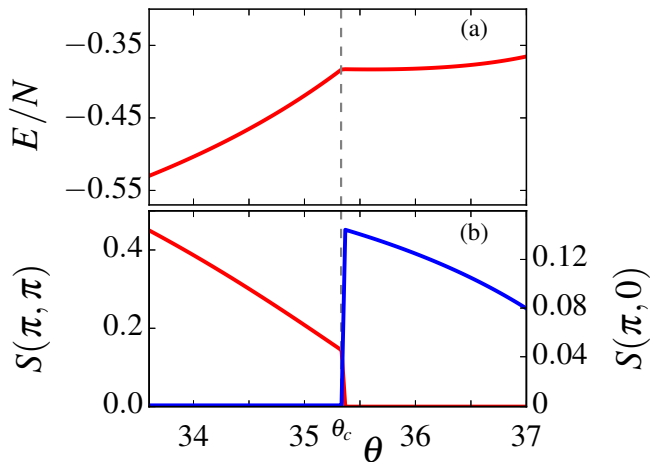


FIG. 10. (a) Energy per particle of the ground state of the dipolar system as a function of the tilt angle θ . There is a discontinuity in the first derivative of the energy around $\theta_c = 35.3^\circ$. The θ values are denoted in units of degrees. (b) Structure factors $S(\pi, \pi)$ (red) and $S(\pi, 0)$ (blue) as a function of the tilt angle θ . Both the quantities show a discontinuous jump at θ_c .

which is a superposition of the checkerboard and striped orders [20, 24]. So, to identify the equilibrium ground state, we use different initial states and consider the converged solution with the lowest energy as the ground state.

2. SSS-CBSS quench dynamics

The quench protocol to study the dynamics of the SSS-CBSS quantum phase transition is

$$\theta(t) = \theta_i - \frac{(\theta_i - \theta_c)}{\tau_Q}(t + \tau_Q). \quad (23)$$

As mentioned earlier, we consider $J = 0.05U$, and $\mu = 0.75U$ for the quench dynamics. Using the above linear quenching protocol, we have $\theta(-\tau_Q) = \theta_i$, and $\theta(0) = \theta_c$. The simulations are performed with $\theta_i = 37^\circ$ and $\theta_f = 32^\circ$, and consider a wide range of the quench times τ_Q . The choice of the parameters are based on the ground state phase diagram of the model Hamiltonian of the system [24]. Like in the J quenching, the quantum fluctuations essential to initiate quantum phase transition are incorporated through the addition of noise to the coefficients in the Gutzwiller wave function.

The density profiles of the system from one of the simulations at different stages of the evolution are shown in Fig. 11. Initially, at the beginning of the quench ($t = -\tau_Q$), the density has striped order. This is shown in the Fig. 11(a). The striped order is, then, altered after the system crosses the critical tilt angle θ_c . The resulting density deformations emerge as patches of checkerboard domains and the system appears like shown in Fig. 11(b). These domains grows in size and the density ordering progresses. At late times, there are large domains of checkerboard order separated by a “network” of remnant striped order as seen in Fig. 11(d).

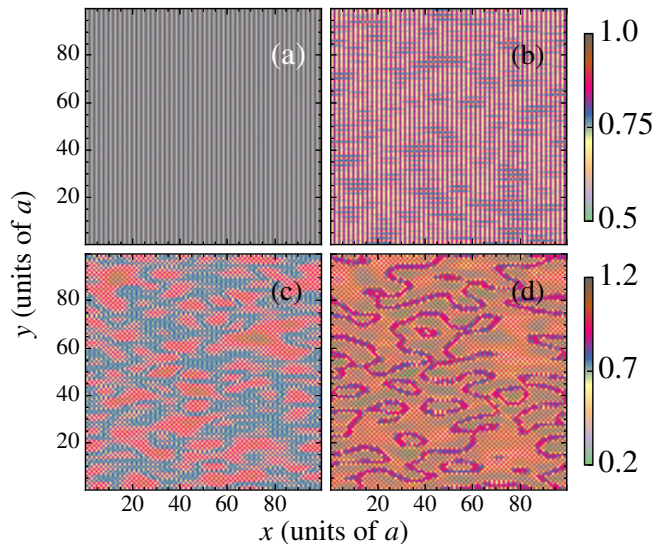


FIG. 11. Snapshots of the density at certain times in the time evolution across SSS-CBSS transition, for $\tau_Q = 20$. The subplot (a) corresponds to the initial state at time $t = -\tau_Q$, (b) corresponds to the state at time $\hat{t} = 44$, (c) denotes the density profile at $t = 50$, and (d) corresponds to the density profile at the end of the quench. We observe domains of checkerboard order emerging at \hat{t} . The density ordering can be noticed from subplots (b)-(d) in the figure.

3. Scaling of \hat{t}

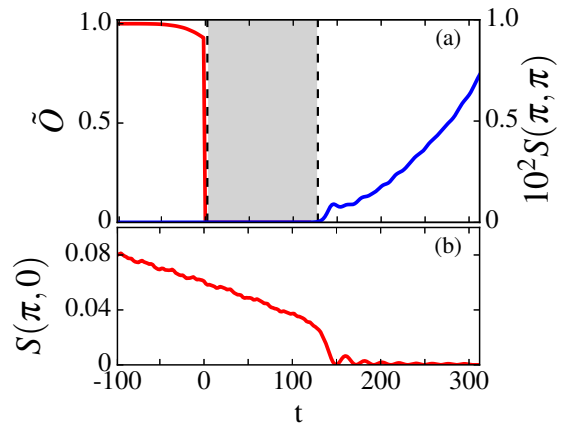


FIG. 12. Overlap \tilde{O} between the ground state and the dynamically evolved state, and the structure factor $S(\pi, \pi)$ as a function of time is shown in (a). The grey shaded region denotes the impulse domain in the dynamics. The time instant \hat{t} , which marks the end of the impulse domain, is when the $S(\pi, \pi)$ becomes non-zero. In (b), we show the $S(\pi, 0)$ as a function of time. There is a decreasing trend in the $S(\pi, 0)$, and near \hat{t} , the decay is steeper.

To identify the end of the adiabatic domain and onset of the impulse domain of the phase transition, we use the overlap \tilde{O} . It is the overlap of the quenched state with the equilibrium ground state having same θ value. The trend of $\tilde{O}(t)$ is as shown in the Fig. 12(a) with the red colored plot. At the early stages, the overlap is close to unit value and this is

representative of the adiabatic evolution. As the quench progresses, it deviates from unity, and becomes zero. This marks the beginning of the impulse domain. Then, the ground state of the system, which has a checkerboard ordering, does not show good fidelity with the quenched state. The time instant when the overlap becomes zero depends on the quench rate, but it is located near θ_c . We expect $\tilde{O}(t)$ to be non-zero when the system leaves impulse domain and re-enters adiabatic domain. However, post impulse domain, the state is populated with topological defects. And, thus this state does not show good fidelity with the corresponding equilibrium ground state. So, $\tilde{O}(t)$ is not a good indicator of the post-impulse adiabatic domain.

To mark the end of the impulse domain, we use $S(\pi, \pi)$ as an indicator. Its trend with time is as shown by the blue color plot in the Fig. 12(a). The $S(\pi, \pi)$ is zero in the SSS phase, but finite in the CBSS phase. Thus, the emergence of the checkerboard order is when $S(\pi, \pi)$ becomes non-zero. In analogy with the J quenching, we mark this time instant as \hat{t} . In other words, there is a time delay in the emergence of the checkerboard order after crossing θ_c . This delay implies the extent of the frozen or the impulse domain of the quench dynamics. In Fig. 12(a), the grey region denotes the impulse domain. As the quench dynamics progresses, the $S(\pi, 0)$ decreases and this trend is discernible from the plot in the Fig. 12(b). This trend continues after crossing the θ_c at $t = 0$, and it arises from the density fluctuations present in the impulse domain. Similar observations were reported in the previous works [69, 70] describing a coarsening dynamics in the impulse domain. Thus, even though the system displays a striped pattern in the impulse domain, the fluctuations cause local density changes, thereby changing the $S(\pi, 0)$. However, after crossing \hat{t} , when the system enters the adiabatic domain, the $S(\pi, 0)$ decreases faster. It becomes zero after some characteristic oscillations as the checkerboard order sets in as the ground state. Another point to note is that there is a finite time interval after \hat{t} , where both the $S(\pi, 0)$ and $S(\pi, \pi)$ are non-zero. That is, post \hat{t} , there are domains of checkerboard order with the striped order as the background, it resembles the emulsion phase [24]. However, as the quench progresses further, the striped pattern diminishes, and the $S(\pi, 0)$ becomes zero.

The scaling of the \hat{t} with τ_Q is shown in the Fig. 13(a). The plot shows the power-law nature of \hat{t} with τ_Q , and the corresponding critical exponent is 0.63. That is, for the SSS-CBSS quantum phase transition $\hat{t} \propto \tau_Q^{0.63}$.

4. Scaling of the Number of domains

One key result of KZM is the scaling of the number of topological defects like vortices N_v or domains N_D . The scaling relation of N_v is given in Eq. (17). However, in the SSS-CBSS transition N_v is not a good choice as the transition is between phases with density or diagonal orders. So, we consider the number of domains N_D , and study the scaling relation with the τ_Q . As a first step, to differentiate the SSS and CBSS domains we introduce a density contrast order parameter

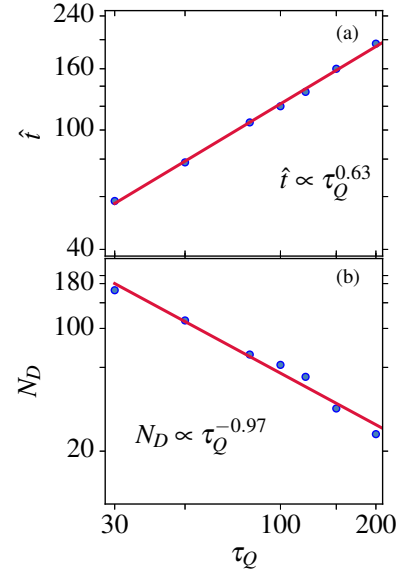


FIG. 13. Scaling of \hat{t} and N_D with τ_Q , for the SSS-to-CBSS phase transition. The power-law scaling of \hat{t} is discernible in (a), and the exponent is 0.63. In (b), the scaling of N_D is presented and the exponent is $d = 0.97$.

ter at the (i, j) lattice site as

$$N_{i,j} = \left| 4\langle n_{i,j} \rangle - (\langle n_{i+1,j} \rangle + \langle n_{i-1,j} \rangle + \langle n_{i,j+1} \rangle + \langle n_{i,j-1} \rangle) \right|.$$

The value of this order parameter is ideally $4(n_A - n_B)$ and $2(n_A - n_B)$ for the checkerboard and striped order, respectively. Hence it serves to contrast between the two ordered phases. As the phases of the quenched states are out-of-equilibrium, $N_{i,j}$ may have a range of values. And, a representative plot is shown in Fig. 14(a). To identify the domains

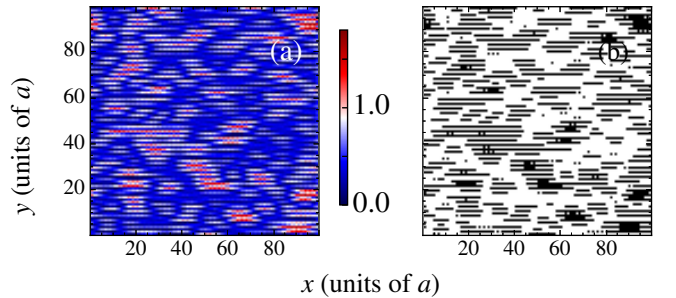


FIG. 14. (a) Plot of the density contrast order parameter $N_{i,j}$. The regions with the values of this order parameter smaller than a certain threshold value correspond to the striped phase, while those with larger values denote the domains of checkerboard order that are formed in the time dynamics. (b) The plot of the distribution of the binary values 0 and -1 , obtained after applying the threshold to the plot (a). The black colored domains indicate those of label 0, while the white regions indicate the domains of label -1 . The domains of the label 0 are counted numerically.

we define a threshold value ϵ of the $N_{i,j}$ and it is set equal to the $N_{i,j}$ of the striped domain. Then the regions with $N_{i,j} > \epsilon$

are considered as CBSS phase and those with lower value as SSS. The lattice sites are, then, labeled as 0 and -1 for the CBSS and SSS phases, respectively. To count the number of domains we use percolation analysis, and the computational algorithms are described in previous works [71, 72]. In the present work, however, we have developed an algorithm based on linked-lists [73]. With this approach a single scan across the system is sufficient to count the domains and label them uniquely. To validate the algorithm, we calculate the N_D for the SDW(1,0)-SSS phase transition. And, we obtain the critical exponent $d = 0.40$, which is in good agreement with the value $d = 0.39$ obtained from the scaling of N_v as shown earlier in the Fig. 9.

In the case of the SSS-CBSS transition, for each value of τ_Q we do an averaging for better statistical description. To do this we select fifteen members at random from the ensemble and then, partition these into three sets. From each set we obtain a value of ϵ by taking average of the prominent striped domains. Using each of the three values we calculate the ensemble average of N_D and take their mean. This statistical averaging provides good representation of the variation of ϵ between the members of the ensemble. Then, the scaling of N_D at \hat{t} with the quench rate $1/\tau_Q$ is analysed and the results are shown in Fig. 13(b). We obtain a power-law scaling with the quench rate, as expected from the KZM. The critical exponent is 0.97. Thus, the quantum phase transition from the striped supersolid to checkerboard supersolid phase obeys the KZ scalings.

V. CONCLUSIONS

In conclusion, we have examined the quantum quench dynamics of the dipolar Bose-Hubbard model in 2D optical lattice. The quenching of the hopping amplitude across the SDW(1,0) - SSS quantum phase transition is studied from the perspective of the KZ mechanism. Specifically, we obtain the power-law scaling of the vortex density, and the correlation length of the system, at time instant \hat{t} , and the critical exponents b and d obey the scaling relation $d = 2b$. Then, the structural quantum phase transition from the striped to the checkerboard supersolid phase is studied by quenching the tilt angle θ . We show the existence of the adiabatic and the impulse domain in this first order phase transition. Then, the domains of checkerboard that gets formed are analysed, and the number of such domains present at time \hat{t} is determined, using the domain counting algorithm based on the linked-lists. The number of domains is shown to obey a power-law scaling behaviour with the quench rate, as expected in KZ mechanism.

ACKNOWLEDGMENTS

The results presented in the paper are based on the computations using Vikram-100, the 100TFLOP HPC Cluster at

Physical Research Laboratory, Ahmedabad, India. S.B acknowledges the support by Quantum Science and Technology in Trento (Q@TN), Provincia Autonoma di Trento, and the ERC Starting Grant StrEnQTh (Project-ID 804305). R.N. further acknowledges DST-SERB for Swarnajayanti fellowship File No. SB/SJF/2020-21/19.

Appendix A: Appendix

Here we comment on the choice of the cutoff Δ , used in generating the random numbers. The value of Δ is fixed by calculating the collective excitations of the equilibrium ground state at initial time. These Bogoliubov-de Gennes (BdG) modes are obtained by adding a fluctuation to the equilibrium ground state [27, 28, 32–34].

$$c_n^{(p,q)}(t) = \left(\bar{c}_n^{(p,q)} + \delta c_n^{(p,q)}(t) \right) e^{-i\omega_0^{(p,q)}t}, \quad (\text{A1})$$

where $\bar{c}_n^{(p,q)}$ corresponds to the equilibrium ground state coefficient, and $\delta c_n^{(p,q)}(t)$ is the fluctuation added to the ground state. The $\omega_0^{(p,q)}$ corresponds to the energy of the unperturbed state at the lattice site (p, q) . To obtain the collective excitations, we use the Bogoliubov approximation and define

$$\delta c_n^{(p,q)}(t) = u_n^{(p,q)} e^{-i\omega t} + v_n^{*(p,q)} e^{i\omega t}, \quad (\text{A2})$$

where ω is the energy of the collective mode, and (u_n, v_n) is the amplitude of the collective mode. The $c_n^{(p,q)}(t)$ are then used in the dynamical Gutzwiller equations, and terms that are linear in the fluctuations part are retained. The resulting set of equations is referred to as the BdG equations. After solving the equations, we obtain the δc_n . Once we obtain δc_n , we use it to calculate the $\delta\langle\hat{n}\rangle$ which correspond to the change in the expectation value of the density. It is given as

$$\delta\langle\hat{n}_{p,q}\rangle = \sum_k k \left(\bar{c}_k^{*(p,q)} \delta c_k^{(p,q)} + \bar{c}_k^{(p,q)} \delta c_k^{*(p,q)} \right). \quad (\text{A3})$$

The order of the magnitude of the $\delta\langle\hat{n}_{p,q}\rangle$ is then used to fix the Δ . For the transition from the SSS to CBSS phase, the calculation of the BdG modes yield $\delta\langle\hat{n}\rangle \approx 10^{-2}$. Thus we accordingly fix the $\Delta \approx 10^{-4}$ so that the $\delta\langle\hat{n}\rangle \approx 10^{-2}$. The same approach is used in fixing the strength of the randomness in the density fluctuations, for the SDW-to-SSS quantum phase transition. Thus we fix the amount of the density fluctuations by studying the collective excitations of the initial equilibrium state.

- [1] T W B Kibble, “Topology of cosmic domains and strings,” *Journal of Physics A: Mathematical and General* **9**, 1387 (1976).
- [2] T.W.B. Kibble, “Some implications of a cosmological phase transition,” *Physics Reports* **67**, 183 (1980).
- [3] W. H. Zurek, “Cosmological experiments in superfluid helium?” *Nature* **317**, 505 (1985).
- [4] W.H. Zurek, “Cosmological experiments in condensed matter systems,” *Physics Reports* **276**, 177 (1996).
- [5] Adolfo del Campo and Wojciech H. Zurek, “Universality of phase transition dynamics: Topological defects from symmetry breaking,” *International Journal of Modern Physics A* **29**, 1430018 (2014).
- [6] Jacek Dziarmaga, “Dynamics of a quantum phase transition and relaxation to a steady state,” *Advances in Physics* **59**, 1063 (2010).
- [7] C. Bäuerle, Yu. M. Bunkov, S. N. Fisher, H. Godfrin, and G. R. Pickett, “Laboratory simulation of cosmic string formation in the early universe using superfluid ^3He ,” *Nature* **382**, 332 (1996).
- [8] V. M. H. Ruutu, V. B. Eltsov, A. J. Gill, T. W. B. Kibble, M. Krusius, Yu. G. Makhlin, B. Plaçais, G. E. Volovik, and Wen Xu, “Vortex formation in neutron-irradiated superfluid ^3He as an analogue of cosmological defect formation,” *Nature* **382**, 334 (1996).
- [9] Isaac Chuang, Ruth Durrer, Neil Turok, and Bernard Yurke, “Cosmology in the laboratory: Defect dynamics in liquid crystals,” *Science* **251**, 1336 (1991).
- [10] Mark J. Bowick, L. Chandar, E. A. Schiff, and Ajit M. Srivastava, “The cosmological kibble mechanism in the laboratory: String formation in liquid crystals,” *Science* **263**, 943 (1994).
- [11] R. Monaco, J. Mygind, R. J. Rivers, and V. P. Koshelets, “Spontaneous fluxoid formation in superconducting loops,” *Phys. Rev. B* **80**, 180501 (2009).
- [12] Shi-Zeng Lin, Xueyun Wang, Yoshitomo Kamiya, Gia-Wei Chern, Fei Fan, David Fan, Brian Casas, Yue Liu, Valery Kiryukhin, Wojciech H. Zurek, and Sang-Wook Batista, Cristian D. and Cheong, “Topological defects as relics of emergent continuous symmetry and higgs condensation of disorder in ferroelectrics,” *Nature Physics* **10**, 970 (2014).
- [13] M. Lewenstein, A. Sanpera, V. Ahufinger, B. Damski, A. Sen(De), and U. Sen, “Ultracold atomic gases in optical lattices: mimicking condensed matter physics and beyond,” *Adv. Phys.* **56**, 243 (2007).
- [14] Christian Gross and Immanuel Bloch, “Quantum simulations with ultracold atoms in optical lattices,” *Science* **357**, 995 (2017).
- [15] M. P. A. Fisher, P. B. Weichman, G. Grinstein, and D. S. Fisher, “Boson localization and the superfluid-insulator transition,” *Phys. Rev. B* **40**, 546 (1989).
- [16] D. Jaksch, C. Bruder, J. I. Cirac, C. W. Gardiner, and P. Zoller, “Cold bosonic atoms in optical lattices,” *Phys. Rev. Lett.* **81**, 3108 (1998).
- [17] M. Greiner, O. Mandel, T. Esslinger, T. W. Hänsch, and I. Bloch, “Quantum phase transition from a superfluid to a Mott insulator in a gas of ultracold atoms,” *Nature (London)* **415**, 39 (2002).
- [18] Markus Greiner, Olaf Mandel, Theodor W. Hänsch, and Immanuel Bloch, “Collapse and revival of the matter wave field of a bose-einstein condensate,” *Nature* **419**, 51 (2002).
- [19] K. Góral, L. Santos, and M. Lewenstein, “Quantum phases of dipolar bosons in optical lattices,” *Phys. Rev. Lett.* **88**, 170406 (2002).
- [20] C Zhang, A Safavi-Naini, Ana Maria Rey, and B Capogrosso-Sansone, “Equilibrium phases of tilted dipolar lattice bosons,” *New Journal of Physics* **17**, 123014 (2015).
- [21] K. Suthar, Hrushikesh Sable, Rukmani Bai, Soumik Bandyopadhyay, Sukla Pal, and D. Angom, “Supersolid phase of the extended bose-hubbard model with an artificial gauge field,” *Phys. Rev. A* **102**, 013320 (2020).
- [22] Kuldeep Suthar, Rebecca Kraus, Hrushikesh Sable, Dilip Angom, Giovanna Morigi, and Jakub Zakrzewski, “Staggered superfluid phases of dipolar bosons in two-dimensional square lattices,” *Phys. Rev. B* **102**, 214503 (2020).
- [23] R. Bai, S. Bandyopadhyay, S. Pal, K. Suthar, and D. Angom, “Bosonic quantum Hall states in single-layer two-dimensional optical lattices,” *Phys. Rev. A* **98**, 023606 (2018).
- [24] Soumik Bandyopadhyay, Rukmani Bai, Sukla Pal, K. Suthar, Rejish Nath, and D. Angom, “Quantum phases of canted dipolar bosons in a two-dimensional square optical lattice,” *Phys. Rev. A* **100**, 053623 (2019).
- [25] S. Pal, R. Bai, S. Bandyopadhyay, K. Suthar, and D. Angom, “Enhancement of the bose glass phase in the presence of an artificial gauge field,” *Phys. Rev. A* **99**, 053610 (2019).
- [26] M. Iskin, “Route to supersolidity for the extended bose-hubbard model,” *Phys. Rev. A* **83**, 051606 (2011).
- [27] Rukmani Bai, Deepak Gaur, Hrushikesh Sable, Soumik Bandyopadhyay, K. Suthar, and D. Angom, “Segregated quantum phases of dipolar bosonic mixtures in two-dimensional optical lattices,” *Phys. Rev. A* **102**, 043309 (2020).
- [28] M. Malakar, S. Ray, S. Sinha, and D. Angom, “Phases and collective modes of bosons in a triangular lattice at finite temperature: A cluster mean field study,” *Phys. Rev. B* **102**, 184515 (2020).
- [29] K. Suthar, Arko Roy, and D. Angom, “Fluctuation-driven topological transition of binary condensates in optical lattices,” *Phys. Rev. A* **91**, 043615 (2015).
- [30] K. Suthar and D. Angom, “Optical-lattice-influenced geometry of quasi-two-dimensional binary condensates and quasiparticle spectra,” *Phys. Rev. A* **93**, 063608 (2016).
- [31] K. Suthar and D. Angom, “Characteristic temperature for the immiscible-miscible transition of binary condensates in optical lattices,” *Phys. Rev. A* **95**, 043602 (2017).
- [32] Konstantin V. Krutitsky, Jonas Larson, and Maciej Lewenstein, “Dark solitons near the mott-insulator–superfluid phase transition,” *Phys. Rev. A* **82**, 033618 (2010).
- [33] Konstantin V. Krutitsky and Patrick Navez, “Excitation dynamics in a lattice bose gas within the time-dependent gutzwiller mean-field approach,” *Phys. Rev. A* **84**, 033602 (2011).
- [34] Takuya Saito, Ipei Danshita, Takeshi Ozaki, and Tetsuro Nikuni, “Detecting the superfluid critical momentum of bose gases in optical lattices through dipole oscillations,” *Phys. Rev. A* **86**, 023623 (2012).
- [35] Oliver Morsch and Markus Oberthaler, “Dynamics of bose-einstein condensates in optical lattices,” *Rev. Mod. Phys.* **78**, 179–215 (2006).
- [36] Chad N. Weiler, Tyler W. Neely, David R. Scherer, Ashton S. Bradley, Matthew J. Davis, and Brian P. Anderson, “Spontaneous vortices in the formation of bose–einstein condensates,” *Nature* **455**, 948 (2008).
- [37] Giacomo Lamporesi, Simone Donadello, Simone Serafini, Franco Dalfovo, and Gabriele Ferrari, “Spontaneous creation of kibble–zurek solitons in a bose–einstein condensate,” *Nature*

- Physics* **9**, 656 (2013).
- [38] S. Donadello, S. Serafini, T. Bienaimé, F. Dalfovo, G. Lamporesi, and G. Ferrari, “Creation and counting of defects in a temperature-quenched bose-einstein condensate,” *Phys. Rev. A* **94**, 023628 (2016).
- [39] L. E. Sadler, J. M. Higbie, S. R. Leslie, M. Vengalattore, and D. M. Stamper-Kurn, “Spontaneous symmetry breaking in a quenched ferromagnetic spinor bose–einstein condensate,” *Nature* **443**, 312 (2006).
- [40] Bogdan Damski and Wojciech H Zurek, “Quantum phase transition in space in a ferromagnetic spin-1 bose–einstein condensate,” *New Journal of Physics* **11**, 063014 (2009).
- [41] Bogdan Damski and Wojciech H. Zurek, “Soliton creation during a bose-einstein condensation,” *Phys. Rev. Lett.* **104**, 160404 (2010).
- [42] M. Anquez, B. A. Robbins, H. M. Bharath, M. Boguslawski, T. M. Hoang, and M. S. Chapman, “Quantum kibble-zurek mechanism in a spin-1 bose-einstein condensate,” *Phys. Rev. Lett.* **116**, 155301 (2016).
- [43] Jérôme Beugnon and Nir Navon, “Exploring the kibble–zurek mechanism with homogeneous bose gases,” *Journal of Physics B: Atomic, Molecular and Optical Physics* **50**, 022002 (2017).
- [44] David Chen, Matthew White, Cecilia Borries, and Brian DeMarco, “Quantum quench of an atomic mott insulator,” *Phys. Rev. Lett.* **106**, 235304 (2011).
- [45] Simon Braun, Mathis Friesdorf, Sean S. Hodgman, Michael Schreiber, Jens Philipp Ronzheimer, Arnau Riera, Marco del Rey, Immanuel Bloch, Jens Eisert, and Ulrich Schneider, “Emergence of coherence and the dynamics of quantum phase transitions,” *Proceedings of the National Academy of Sciences* **112**, 3641 (2015).
- [46] Jin-Ming Cui, Yun-Feng Huang, Zhao Wang, Dong-Yang Cao, Jian Wang, Wei-Min Lv, Le Luo, Adolfo del Campo, Yong-Jian Han, Chuan-Feng Li, and Guang-Can Guo, “Experimental trapped-ion quantum simulation of the kibble-zurek dynamics in momentum space,” *Scientific Reports* **6**, 33381 (2016).
- [47] Jacek Dziarmaga, “Dynamics of a quantum phase transition: Exact solution of the quantum ising model,” *Phys. Rev. Lett.* **95**, 245701 (2005).
- [48] Wojciech H. Zurek, Uwe Dorner, and Peter Zoller, “Dynamics of a quantum phase transition,” *Phys. Rev. Lett.* **95**, 105701 (2005).
- [49] Anatoli Polkovnikov, “Universal adiabatic dynamics in the vicinity of a quantum critical point,” *Phys. Rev. B* **72**, 161201 (2005).
- [50] André Eckardt, Christoph Weiss, and Martin Holthaus, “Superfluid-insulator transition in a periodically driven optical lattice,” *Phys. Rev. Lett.* **95**, 260404 (2005).
- [51] A. G. Green and S. L. Sondhi, “Nonlinear quantum critical transport and the schwinger mechanism for a superfluid-mott-insulator transition of bosons,” *Phys. Rev. Lett.* **95**, 267001 (2005).
- [52] Keita Shimizu, Yoshihito Kuno, Takahiro Hirano, and Ikuo Ichinose, “Dynamics of a quantum phase transition in the bose-hubbard model: Kibble-zurek mechanism and beyond,” *Phys. Rev. A* **97**, 033626 (2018).
- [53] Keita Shimizu, Takahiro Hirano, Jonghoon Park, Yoshihito Kuno, and Ikuo Ichinose, “Out-of-equilibrium dynamics of multiple second-order quantum phase transitions in an extended bose-hubbard model: Superfluid, supersolid, and density wave,” *Phys. Rev. A* **98**, 063603 (2018).
- [54] Yijia Zhou, Yongqiang Li, Rejish Nath, and Weibin Li, “Quench dynamics of rydberg-dressed bosons on two-dimensional square lattices,” *Phys. Rev. A* **101**, 013427 (2020).
- [55] Keita Shimizu, Takahiro Hirano, Jonghoon Park, Yoshihito Kuno, and Ikuo Ichinose, “Dynamics of first-order quantum phase transitions in extended bose–hubbard model: from density wave to superfluid and vice versa,” *New Journal of Physics* **20**, 083006 (2018).
- [56] Ivan B. Coulamy, Andreia Saguia, and Marcelo S. Sarandy, “Dynamics of the quantum search and quench-induced first-order phase transitions,” *Phys. Rev. E* **95**, 022127 (2017).
- [57] L.-Y. Qiu, H.-Y. Liang, Y.-B. Yang, H.-X. Yang, T. Tian, Y. Xu, and L.-M. Duan, “Observation of generalized kibble-zurek mechanism across a first-order quantum phase transition in a spinor condensate,” *Science Advances* **6** (2020), 10.1126/sciadv.aba7292.
- [58] H-Y Liang, L-Y Qiu, Y-B Yang, H-X Yang, T Tian, Y Xu, and L-M Duan, “Observation of heat scaling across a first-order quantum phase transition in a spinor condensate,” *New Journal of Physics* **23**, 033038 (2021).
- [59] S. Yi, T. Li, and C. P. Sun, “Novel quantum phases of dipolar bose gases in optical lattices,” *Phys. Rev. Lett.* **98**, 260405 (2007).
- [60] Ipeei Danshita and Carlos A. R. Sá de Melo, “Stability of superfluid and supersolid phases of dipolar bosons in optical lattices,” *Phys. Rev. Lett.* **103**, 225301 (2009).
- [61] Huan-Kuang Wu and Wei-Lin Tu, “Competing quantum phases of hard-core bosons with tilted dipole-dipole interaction,” *Phys. Rev. A* **102**, 053306 (2020).
- [62] S. Baier, M. J. Mark, D. Petter, K. Aikawa, L. Chomaz, Z. Cai, M. Baranov, P. Zoller, and F. Ferlaino, “Extended bose-hubbard models with ultracold magnetic atoms,” *Science* **352**, 201–205 (2016).
- [63] D. S. Rokhsar and B. G. Kotliar, “Gutzwiller projection for bosons,” *Phys. Rev. B* **44**, 10328 (1991).
- [64] K. Sheshadri, H. R. Krishnamurthy, R. Pandit, and T. V. Ramakrishnan, “Superfluid and insulating phases in an interacting-boson model: Mean-field theory and the RPA,” *EPL* **22**, 257 (1993).
- [65] Bogdan Damski, “The simplest quantum model supporting the kibble-zurek mechanism of topological defect production: Landau-zener transitions from a new perspective,” *Phys. Rev. Lett.* **95**, 035701 (2005).
- [66] Bogdan Damski and Wojciech H. Zurek, “Adiabatic-impulse approximation for avoided level crossings: From phase-transition dynamics to landau-zener evolutions and back again,” *Phys. Rev. A* **73**, 063405 (2006).
- [67] A. J. Leggett, “Can a solid be superfluid?” *Phys. Rev. Lett.* **25**, 1543 (1970).
- [68] T. Ohgoe, T. Suzuki, and N. Kawashima, “Quantum phases of hard-core bosons on two-dimensional lattices with anisotropic dipole-dipole interaction,” *Phys. Rev. A* **86**, 063635 (2012).
- [69] Giulio Biroli, Leticia F. Cugliandolo, and Alberto Sicilia, “Kibble-zurek mechanism and infinitely slow annealing through critical points,” *Phys. Rev. E* **81**, 050101 (2010).
- [70] Kangeun Jeong, Bongsoo Kim, and Sung Jong Lee, “Growth kinetics of the two-dimensional ising model with finite cooling rates,” *Phys. Rev. E* **99**, 022113 (2019).
- [71] J. Hoshen and R. Kopelman, “Percolation and cluster distribution. i. cluster multiple labeling technique and critical concentration algorithm,” *Phys. Rev. B* **14**, 3438 (1976).
- [72] Nanako Shitara, Shreya Bir, and P Blair Blakie, “Domain percolation in a quenched ferromagnetic spinor condensate,” *New Journal of Physics* **19**, 095003 (2017).
- [73] Hrushikesh Sable, Deepak Gaur, and D. Angom, under preparation.